Multi-Functional Double Mode Inverter for Power Quality Enhancement in Smart-Grid Applications

F. Harirchi, *Student Member, IEEE*, M. Godoy. Simões, *Fellow, IEEE*, M. Babakmehr, *Student Member, IEEE*, A. AlDurra *Senior Member, IEEE*, S.M. Muyeen, *Senior Member, IEEE, A.Bubshait*[1]

***Abstract* – This paper introduces a new multi-functional double mode inverter (MFDMI) scheme, which is able to operate under a variety of operational conditions for aggregation of PV-based renewable energy resources. Detecting islanded situation within a new and fast approach, regulating the voltage in the islanded mode, smooth transition between islanded and grid-tied (GT) modes, injecting both active and reactive powers to the grid in addition to compensating the harmonics from nonlinear loads are beyond the most notable functionalities of the proposed framework. Technically, we exploit a combinational control scheme formed by instantaneous power theory, vector-control and a proportional integral resonant (PIR) controller to address the required functionalities. To deal with the low output power issue, photovoltaic (PV) cells are aggregated through a high gain DC-DC floating interleaved boost converter (FIBC). Moreover, a battery back-up module with bidirectional DC-DC floating interleaved buck-boost converter (FIBBC) is used to improve the system reliability and dispatch ability. The effectiveness of the proposed framework has been first verified within a comprehensive PSIM simulation results and then has been examined under realistic situations using the real-time simulator OPAL-RT with DSP modules (hardware in the loop) for a broad range of conditions and within different practical scenarios.**

***Index Terms*-- Multi-functional double mode inverter, Smooth transition, PV-based Microgrid, Unified controller, Smartgrid, Islanded detection, Harmonic compensation.**

I. INTRODUCTION

Electricity generation based on renewable energy sources (RES) such as PVs, wind turbines, and geothermal is efficient, reliable, and environmentally friendly. RESs are usually available in a cluster, defined as a microgrid, i.e. normally connected to grid and capable to negotiate with the grid by injecting/absorbing power [1]-[3]. Grid-Tied Inverters (GTI) are popular power electronic interfaces (PEI) connecting RES to the grid with high reliability, excellent power quality and intelligence. However, an important technical challenge is adaption of a microgrid to work as an individual system in case of faulty situations (Islanded mode). In such a configuration the corresponding inverter is called a double-mode inverter [18]. Another important concern regarding aggregation of microgrids is the harmonic injection issue. These unwanted phenomena are injected to the grid by PEIs, nonlinear loads, and fluctuation in output power of RES. Recently, active filtering-based harmonic compensation techniques have found lots of interests [4]. In most of the active filtering studies [4]-[7], an individual inverter with additional controller and an extra battery source are needed to operate in parallel with the main inverter to moderate the harmonic effect [7]. An LCL filter has been used in the output stage of the GT inverters and active filters, instead of conventional low order L or LC filters, in order to improve output current waveforms [8]-[10].

In order to reduce the system configuration complexity and size, a new category of GTIs have been developed in [11]-[14] widely known as Multi-Functional GTIs (MFGTI). Recently, a coordinated control of multiple MFGTIs is presented and verified by experimental results in [14]. In [15], a multi-objective optimal compensation strategy is presented for 3H-bridge MFGTI application. However, most of the aforementioned methods suffer from different technical-practical restrictions [11]. More recently a new MFGTI configuration has been developed in [11], however, an extra procedure is needed to calculate the comprehensive power quality index in order to adjust the inverter reference currents. Moreover, the system configuration has been only realized under grid connected mode. The importance of MFGTI in addition to a literature review of the state of the art in MFGTI can be found in [11]. Besides system complexity and extra required hardware or software modules, the major drawback with most of the aforementioned methods is their single modality, where the islanded mode has not been considered as an operational mode. Besides, some articles are considering the isolated microgrids as well [1].

Some works have been developed for two operational modes [16]-[19], However, in most of these articles the harmonic compensation [24], reliable Islanded detection and the inherent mode transition instability have not been addressed. For example, in [18] PI controllers are used for current stabilization in GT mode, however, harmonical current components cannot be appropriately compensated in this way. Also in [19], the harmonic compensation has been addressed with a simple LC output filter which is not reliable in real experimental cases. Another drawback regarding these approaches is that they mainly use separated controllers for each operational mode. There are also some other works which have not been directed in case of PV-based system so, do not account for the related practical challenges [1].

In this paper the authors aim to address the aforementioned issues by describing a *multifunctional double mode* inverter (MFDMI) capable of injecting the power generated by RESs and also compensate harmonics of nonlinear loads, enhancing the power quality at the point of common coupling (PCC), detecting islanded situation and control the voltage at PCC in islanded mode [20]-[21]. We proposed a unified controller approach to control the inverter in both operating modes simultaneously with an optimal and fast transition scheme. Initial studies made by the authors have been reported in [17]. Further design studies were introduced in this current paper, where a novel synchronous reference frame transformation-

[1] F. Harirchi, M.G. Simões, M. Babakmehr, A. Bubshait, are with the EECS Dept, Colorado School of Mines, Golden, CO, USA, (e-mails:{harirchi, msimoes, mbabakme} @ mines.edu). A. AlDurra and SM. Muyeen from Petroleum Institute, Abu Dhabi (emails: {aaldurra, smmuyeen} @pi.ac.ae).

978-1-4799-8397-1/16/$31.00 © 2016 IEEE

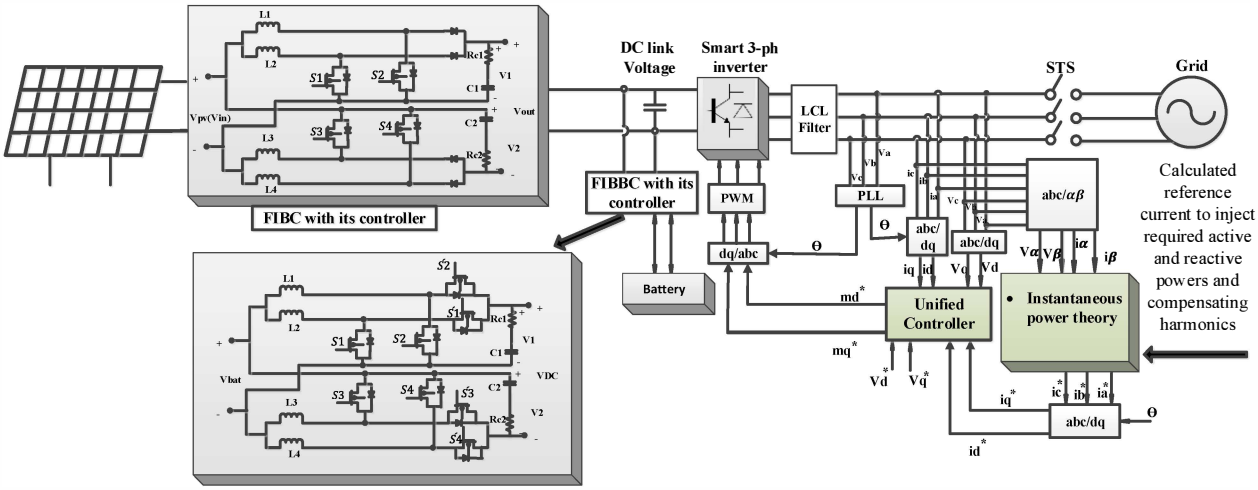

Fig.1. Multi-functional double mode inverter for PV-based microgrid

based method is developed to detect the fault near real time and switch the system from the GT to islanded (and vice-versa). Technically, we exploit a combinational control scheme formed by instantaneous power theory, vector-control and a proportional integral resonant (PIR) controller to address the required functionalities. This inverter is designed to be used as a smart interface for microgrids, contributing for the technology of smart-grids. The system diagram of the proposed MFDMI is shown in Fig. 1. To deal with the low output voltage issue, photovoltaic (PV) cells are aggregated through a high gain FIBC [16]. Moreover, a battery back-up module with bidirectional DC-DC FIBBC [16], [27] is used to improve the system reliability and dispatch ability. The effectiveness of the proposed framework has been first verified within a comprehensive PSIM simulation results and then has been examined under realistic situations using the real-time simulator OPAL-RT with DSP modules, as hardware in loop, for a broad range of conditions and within different practical scenarios. This article is structured as follows: in Section II, the operational modes and corresponding functionalities of the MFDMI are introduced. In Section III a control algorithm for the MFDMI with smooth transition between GT and islanded modes in addition to *instantaneous* Islanded detection algorithm will be presented. Finally, Section IV contains simulation results and Section V contains our conclusions.

II. Multi-Functional Double-Mode Inverter

The proposed inverter is the core part of the microgrid with main features called as operational modes. The operating modes for the proposed MFDMI are described below.

A. Grid-connected mode / Current control mode

The most important functionalities in GT mode includes: 1) controlling the output current of the MFDMI at PCC in order to negotiate with the main grid by injecting active and reactive powers, and 2) compensating harmonics of the nonlinear loads, in addition to the power fluctuations of RESs. In this work the instantaneous power theory (p-q theory) [22], is used in order to adjust the reference value of the currents according to the grid's demand. Based on PV generated power, in addition to load-grid requirements, the proposed MFDMI can operated within the following eight (sub-modes) functionalities:

- Harmonic compensation and reactive power injection
- Harmonic compensation and active power injection
- Active power injection
- Reactive power injection
- Active and reactive power injection
- Harmonic compensation
- Active and reactive power injection and harmonic compensation
- Store the PV module energy into the battery

B. Islanded mode / Voltage control mode

In the Islanded mode since the grid is disconnected from the microgrid, the voltage stability is considered as the main purpose. Accordingly, the main objective of the controller is to control the PCC voltage magnitude and frequency, which is called the grid forming mode.

C. Transition Mode

The transition procedure between two aforementioned main operational modes can be considered as a third pseudo mode; also called the transient operational mode. The main objective within this mode is to perform a smooth transition avoiding unwanted transient effects on the system operation.

In the transition phase, synchronization is the most important issue. A unified control approach has been implemented in this paper to solve the transition problem. The corresponding current controller in the GT mode and the voltage controller in the islanded mode are combined as a unified controller to provide a smooth transition for MFDMI. Full details are described in Section III.

III. Proposed Control Scheme

In this section we will first describe the control strategy in the GT mode within parts A to C. Next, we will discuss the

control strategy for the islanded mode in parts C and D. Finally, we will end up with describing the unified smooth transition algorithm in part E.

A. Grid Negotiation (Active and Reactive power injection)

As mentioned in Section II, the main functionalities in GT mode are controlling injected active and reactive powers as well as harmonic compensation. In order to inject an specified amount of active and reactive powers named P_{ref} and Q_{ref}, respectively, the corresponding reference values for the (namely) active i_{d2}^{*} and reactive i_{q2}^{*} currents are calculated from (1)-(2), Fig.3, where, P_{ref} and Q_{ref} can be determined by an energy management system according to the selling price of active and reactive power to the grid.

$$P_{ref} = \frac{3}{2}\left(v_d {i_{d2}}^{*} + v_q {i_{q2}}^{*}\right) \quad (1)$$

$$Q_{ref} = \frac{3}{2}\left(v_q {i_{d2}}^{*} - v_d {i_{q2}}^{*}\right) \quad (2)$$

where v_d and v_q are the representation of the 3-phase voltages in the famous rotating reference frame basis (d-q) [17].

B. p-q theory for harmonic compensation in GT

The instantaneous power theory or p-q theory is introduced by Akagi and used to control active filters in [22]. In this work we adjusted this method to be used for harmonic component compensation. Since the p-q theory works in the time-domain, it allows the control strategy to be defined within a near real time approach. Roughly speaking, we utilized the p-q theory as a signal decomposition method in the proposed MFDMI. This theorem consists of an algebraic transformation (Clarke transformation) of the three-phase voltages and currents in the a-b-c coordinates to the α-β-0 coordinates (3)-(4), followed by the calculation of the instantaneous power components (5):

$$\begin{bmatrix} v_a \\ v_b \\ v_c \end{bmatrix} = \sqrt{\frac{2}{3}} \begin{bmatrix} 1 & 0 \\ -\frac{1}{2} & \frac{\sqrt{3}}{2} \\ -\frac{1}{2} & -\frac{\sqrt{3}}{2} \end{bmatrix} \begin{bmatrix} v_\alpha \\ v_\beta \end{bmatrix}, \begin{bmatrix} i_a \\ i_b \\ i_c \end{bmatrix} = \sqrt{\frac{2}{3}} \begin{bmatrix} 1 & 0 \\ -\frac{1}{2} & \frac{\sqrt{3}}{2} \\ -\frac{1}{2} & -\frac{\sqrt{3}}{2} \end{bmatrix} \begin{bmatrix} i_\alpha \\ i_\beta \end{bmatrix} \quad (3)$$

$$\begin{bmatrix} v_\alpha \\ v_\beta \end{bmatrix} = \sqrt{\frac{2}{3}} \begin{bmatrix} 1 & -\frac{1}{2} & -\frac{1}{2} \\ 0 & \frac{\sqrt{3}}{2} & -\frac{\sqrt{3}}{2} \end{bmatrix} \begin{bmatrix} v_a \\ v_b \\ v_c \end{bmatrix}, \begin{bmatrix} i_\alpha \\ i_\beta \end{bmatrix} = \sqrt{\frac{2}{3}} \begin{bmatrix} 1 & -\frac{1}{2} & -\frac{1}{2} \\ 0 & \frac{\sqrt{3}}{2} & -\frac{\sqrt{3}}{2} \end{bmatrix} \begin{bmatrix} i_a \\ i_b \\ i_c \end{bmatrix} \quad (4)$$

$$\begin{bmatrix} p \\ q \end{bmatrix} = \begin{bmatrix} v_\alpha & v_\beta \\ v_\beta & -v_\alpha \end{bmatrix} \begin{bmatrix} i_\alpha \\ i_\beta \end{bmatrix}, \quad (5)$$

where p is the instantaneous real power (which corresponds to the energy per time unit that is transferred from the power supply to the load), and q is the instantaneous imaginary power, which corresponds to the power that is exchanged between different phases of the load. We can decompose each term p and q to their mean and oscillating parts as follows:

$$p = \tilde{p} + \overline{p} \quad (6)$$

$$q = \tilde{q} + \overline{q}, \quad (7)$$

where $\overline{p}$ is the average component (desired power component) and $\overline{q}$ (which is the average value of the instantaneous imaginary power) is equal to the conventional reactive power. For balanced voltage sources, the oscillating powers $\tilde{p}$ and $\tilde{q}$ represent the undesirable powers due to harmonic components in the load current. The oscillating parts of the real and imaginary powers are caused by harmonics, and they must be compensated by the MFDMI. The corresponding current components, which are needed to be compensated[2] by MFDMI, can be calculated in a stationary reference frame (α-β) as follows:

$$\begin{bmatrix} i_{\alpha 1}^{*} \\ i_{\beta 1}^{*} \end{bmatrix} = \frac{1}{{v_\alpha}^2 + {v_\beta}^2} \begin{bmatrix} v_\alpha & v_\beta \\ v_\beta & -v_\alpha \end{bmatrix} \begin{bmatrix} \tilde{p} \\ \tilde{q} \end{bmatrix}, \quad (8)$$

where $i_{\alpha 1}^{*}$ and $i_{\beta 1}^{*}$ are the harmonic parts of the current in α and β axis, that should be compensated (generated) by MFDMI, respectively. Since the current control scheme is built based on the d-q control framework (next section), compensated current components should be converted from the stationary reference frame (α-β) to the rotating reference frame (d-q) by using:

$$\begin{bmatrix} i_{d1}^{*} \\ i_{q1}^{*} \end{bmatrix} = \begin{bmatrix} cos(\theta) & sin(\theta) \\ -sin(\theta) & cos(\theta) \end{bmatrix} \times \begin{bmatrix} i_{\alpha 1}^{*} \\ i_{\beta 1}^{*} \end{bmatrix}, \quad (9)$$

where i_{d1}^{*} and i_{q1}^{*} are the harmonic parts of current in d and q axis, respectively. The proposed algorithm for calculating the compensating currents is shown in Fig. 2.

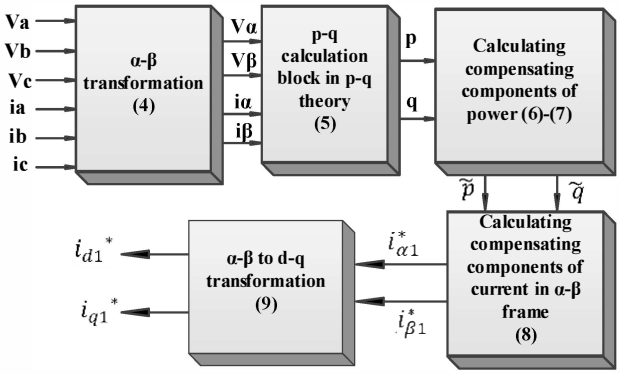

Fig.2. Algorithm to find harmonic components for harmonic compensation by using p-q theory

C. d-q based PIR control scheme in GT Mode

Once the grid currents are decomposed by the p-q theory (Fig.2), the oscillating parts of the instantaneous real and imaginary powers are defining the compensating currents (8). As mentioned before, these components are converted to a stationary domain (d-q frame i_{d1}^{*} and i_{q1}^{*}), (9), and added to the ${i_{d2}}^{*}$ and ${i_{q2}}^{*}$ (Fig.3) to make the final reference values for the current controller as shown in Fig. 3.

[2] For sake of clarity we should mention that: the "harmonic" component of the current from load perspective is equal to the component that should be "compensated" from the MFDMI viewpoint, so these two phrases have been used interchangeably.

$$I_{dref} = {i_{d1}}^* + {i_{d2}}^* \quad (10)$$
$$I_{qref} = {i_{q1}}^* + {i_{q2}}^* \quad (11)$$

A regular PI controller has a good performance in controlling DC parameters. Therefore, in case of linear loads, (since I_{dref} and I_{qref} are DC parameters) the PI controller can be used as an appropriate option. However, in case of nonlinear loads, the harmonic components of the current waveform changes the I_{dref} and I_{qref} to AC parameters. Thus, in this case the PI controller cannot operate adequately. As a result, in this work a proportional-integral-resonant (PIR) controller (which is a combination of a PI and PR controllers) is implemented to control the current loop. The most important PIR control feature is its ability to track both DC and AC quantities at the same time [23]. Roughly speaking, in a PIR configuration, the PI part controls DC current components in d-q axis to follow the desired active and reactive power injection to the grid, while the resonant part controls AC current components in d-q axis, which are caused because of the presence of harmonics. The overall combination guarantees an accurate tracking of DC and AC currents components.

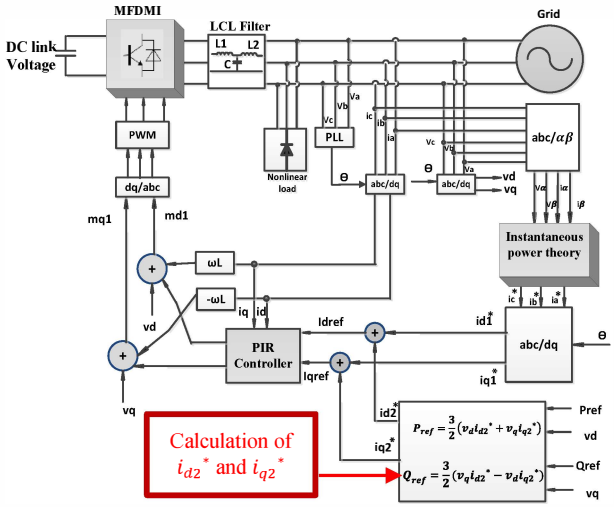

Fig.3. Current control diagram in the GT mode

Under distorted grid current conditions (in presence of a 3-phase diode rectifier), if the angular frequency of the system is ω, which is calculated by a phase locked loop (PLL), the current in the d-q reference frame contains DC values of the positive sequence from the fundamental component in addition to AC terms caused by harmonic components of -5ω and 7ω. An important point is that the generalized AC resonant term (R) is a two-sided integrator operator. This means that having a resonant part adjusted at the angular frequency of 6ω, we are able to nullify the error for the positive sequence at both of the positive and negative frequencies of 6ω and -6ω simultaneously. Similarly, the zero steady state error of DC components can be achieved by the usage of the standard PI controllers. A resonant regulator can be adjusted at the 6ω frequency value (in the current controller) resulting in a decreased error of the AC signal (with the frequencies of $\pm 6\omega$). Therefore, a PIR current controller in the d-q reference frame can be developed for directly regulating both the positive sequence of the fundamental component and the harmonic components of -5ω and 7ω.

$$G_{PIR} = K_p + \frac{K_I}{s} + \frac{K_R\, s}{s^2+\omega_R{}^2}, \quad (12)$$

Fig.4 shows a block diagram of the designated PIR controller in d and q frames. The general transfer function of a typical PIR controller is defined as follows:

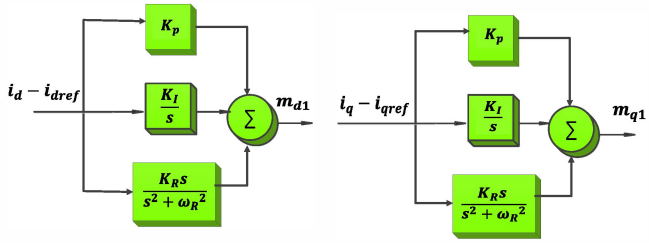

Fig.4. Schematic of PIR controller

where K_p is a proportional gain and K_I plays the same role as that in the regular PI controller, which basically controls the system dynamics such as bandwidth and system marginal parameters (gain and phase). Moreover, the resonant control term K_R provides an infinite gain at the frequencies of $\pm 6\omega$ in order to address the corresponding issues within the AC components. In our configuration m_{d1} and m_{q1} represent the output current control signals of the PIR controller. In the GT mode the final control signals in d and q frames are calculated as follows:

$$m_{q1} = \left(I_{qref} - i_q\right)\left(K_p + \frac{K_I}{s} + \frac{K_R\, s}{s^2+\omega_R{}^2}\right) + \omega L + v_q \quad (13)$$
$$m_{d1} = \left(I_{dref} - i_d\right)\left(K_p + \frac{K_I}{s} + \frac{K_R\, s}{s^2+\omega_R{}^2}\right) - \omega L + v_d \quad (14)$$

where L ($L = L_1 + L_2$) is the equivalent LCL filter inductance. The PIR controller terms have been optimized based on the experimental results as follow: K_p =15, K_I = 103, and K_R = 24. Once the controlling signals m_{q1} and m_{d1} are calculated, the park inverse transformation [25] is applied to convert them back into a-b-c coordinates. The final control signals are applied to the PWM.

D. Islanded detection

Islanded mode detection is classified as a challenging issue in microgrid technology. Due to system sensitivity (in case of critical loads), an *instantaneous* fault (islanded situation) detection is a critical task in microgrids. Two major factors should be considered in Islanded detection procedure: 1) detection time and 2) serious level of the fault. Due to variations and measurement noise in a sample recorded sinusoidal voltage signal, the original time domain representation-based frameworks (such as RMS value) may not be appropriate to define a trustable and fast fault detection criterion. In order to address this issue, we suggest an

instantaneous islanded detection framework by using instantaneous rotating reference frames [25]. Once the voltage at the grid side is measured it is converted into d-q frames (which are DC values in nature) and compared with the reference values of the grid voltage in d-q frame (in this paper we assumed that the d axis is perfectly aligned on the grid voltage):

$$\begin{cases} v_{aref} = 120\angle 0^0 \\ v_{dref} = 120V = 1pu \\ v_{qref} = 0pu \end{cases} \quad (15).$$

Once a fault occurs in the grid, the grid's voltage becomes distorted. Distorted voltage can happen in different formats (such as, voltage sag, voltage swell, over voltage, under voltage and interruption). In all of these cases, the d and q components of the grid voltage are changed accordingly. Running variety of faulty simulated cases, we concluded that the best choice for faulty limits on d and q components are 0.95pu and 1.05pu. Therefore, at each time instance if v_d or v_q are happened to be less than 0.95pu or more than 1.05pu, the inverter recognizes that the fault in the grid or a sever power quality event is happened, therefore the static transfer switch (STS) is opened and finally the operating mode is changed to the islanded mode. The detailed version of this algorithm will be presented in the future works.

E. d-q based PI Control scheme in Islanded Mode

The proposed voltage control block in islanded mode has been shown in Fig.5. In the islanded mode the microgrid is disconnected from the main grid, thus the main objective of the controller is to adjust the voltage magnitude and frequency in adequate levels for local loads. Since d and q components of voltages appear as DC components, the PI controller is adequate for stabilization in this mode. The corresponding d and q components are shown by m_{d2} and m_{q2}, respectively. The PI controller terms have been optimized based on the experimental results as follow: $K_p = 11$, and $K_I = 120$.

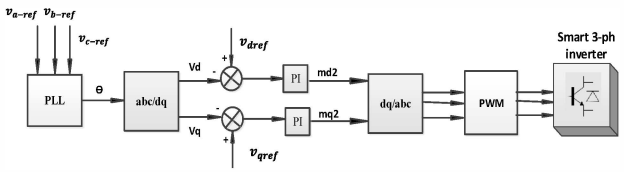

Fig.5. Voltage control diagram in the islanded mode.

F. Unified control Scheme for Smooth Transition

Fig.6 illustrates the proposed smooth transition algorithm between the GT and islanded modes. Based on the defined control rules in this algorithm, once the operating mode is changed to Islanded mode the system dominant control rule should be changed into voltage control. In the Islanded mode the reference values for voltages are set to $v_{dref} = 1pu$ and $v_{qref} = 0pu$, respectively. In this condition since the STS is open the actual injected current to the grid is zero, as a result, by setting the reference values of current components (I_{dref} and I_{qref}) to zero, the output control signal of the current controller will be zero (m_{d1}= $m_{q1} = 0$) as well, and the voltage controller becomes the dominant controller. Once the grids' problem is solved, the STS is closed so the microgrid is reconnected to the main grid. Synchronization is the most important issue in this case. In this work the synchronization is provided by a conventional synchronous reference frame PLL [18]. In the GT mode, injected power to the grid is controlled by the controlling the current quality and quantity. In this mode since the PCC voltage is equal to the grid voltage (which is the reference voltage), the output of the voltage controller is zero (m_{d2}= $m_{q2} = 0$). Thus, the current controller is the dominant controller. Finally, adding the output of the current controller with the output of the voltage controller, and applying the resulted control signal into the PWM, a very smooth transition between the two modes can be achieved. Fig.6. shows the proposed control algorithm for the MFDMI, where $m_d{}^*$ *and* $m_q{}^*$are the final output control signals of the unified controller that are inserted into PWM by using dq/abc transformation.

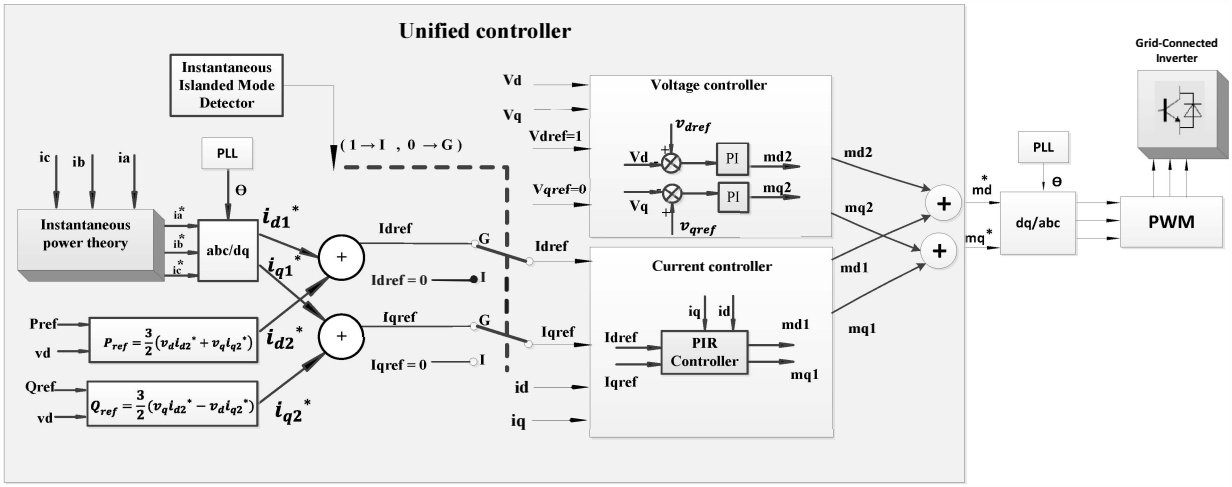

Fig.6. Unified Control algorithm for MFDMI with a smooth transition between two main operational modes

IV. Simulation Results and Experimental Work

The proposed MFDMI within the corresponding microgrid configuration (Fig.1) has been initially modelled in PSIM software and then the electrical configuration of the system implemented through the experimental platform which is illustrated in Fig.7. The analysis of FIBC and FIBBC have been fully described in our previous work [16] and experimentally developed in the ACEPS lab in Colorado School of Mines. Moreover, a full hardware setup for a PV-based system is under development (Fig.7). It is shown that the proposed system can satisfy the IEEE-std-519 and IEEE-std-1547.4 for microgrids.

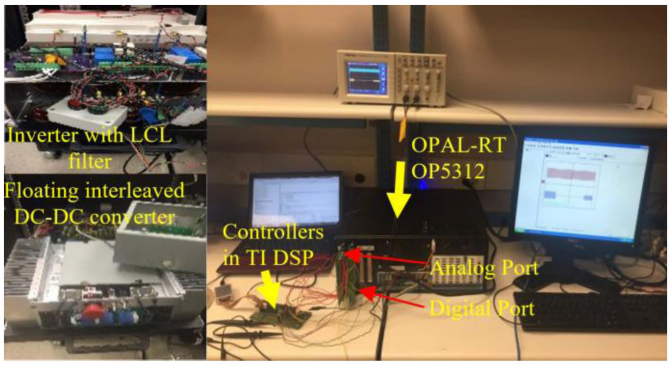

Fig.7. Experimental test bench.

A. Simulation Results in PSIM

This section contains simulation results for the proposed MFDMI under variety of practical conditions. On the DC side PV modules are connected to the DC link through a DC-DC FIBC. Moreover, an energy storage unit is aggregated to the overall system with a FIBBC to increase the reliability of the overall system. Parameters of the proposed inverter are listed in Table I. In order to verify the performance of the designed system, different case studies were considered where the full length corresponding grid current vs time is illustrated in Fig. 8. We will discuss these situations using the following case studies. All of the corresponding results have been illustrated for phase a (similar results were observed for phase b and c).

TABLE I: Parameters of the Inverter

Input voltage	$Vdc = 400$
Output voltage (1Φ)	$Vout = 120Vrms$
Inductor of LCL	$L_1 = 2.33mH$ (inverter side) L_2 =0.045mH (grid side)
Capacitor of LCL	$C = 5e-6F$
Switching frequency	$f_s = 12KHz$
Frequency of the grid	f_g=60Hz
Inverter nominal power	5 kVA

Case 1: In this case, at t=0.1s, a nonlinear load (a 3-phase diode rectifier with 5A DC current source) is added to the PCC. The corresponding current waveform of the nonlinear load is shown in Fig.9.a. The compensating current term (calculated by p-q theory) is shown in Fig.9.b. Finally, the compensated grid current, in presence of the nonlinear load is shown in Fig.9.c.

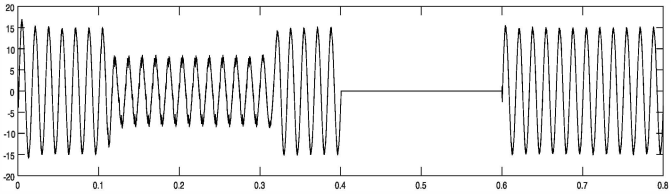

Fig. 8. Injected current to grid in different operational conditions of MFDMI

We can see that, in the presence of the nonlinear load in the system, the controller compensates harmonic terms, and the THD of the grid current remains under 2%. After 0.3s, the nonlinear load is removed, where the controllers' fast response to this load change is observed from Fig.9.c.

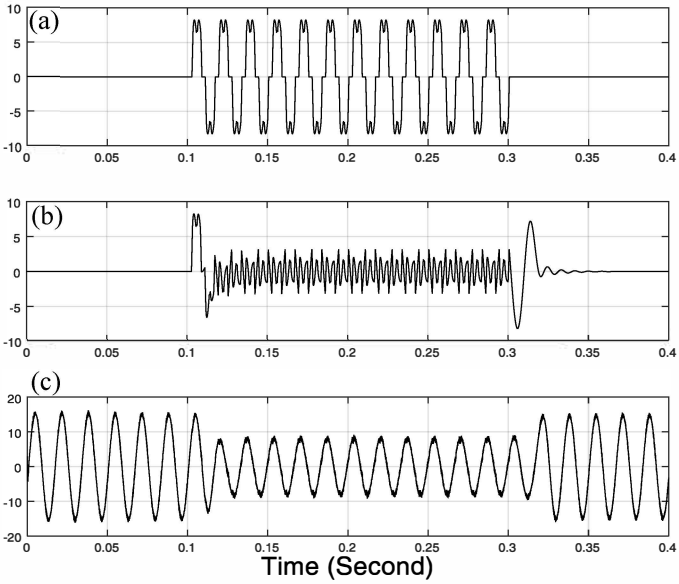

Fig. 9. a) Current of nonlinear load b) Compensating current calculated by p-q theory c) Compensated grid current after adding nonlinear load at 0.1s, and removing nonlinear load at 0.3s

Case 2: Using the proposed instantaneous islanded detection approach, a fault is detected in the grid at t=0.4s. As a result the controller changes the STS status to the open position and the inverter switches to islanded mode. In this case according to the proposed algorithm in Section III.E, the voltage controller adjusts the PCC voltage and does not have any control on the injected power to the grid. Fig. 8 and Fig. 10.a show the grids' current and PCC voltage for the islanded mode duration (0.4-0.6s), respectively. As it can be seen, the controller has a good performance with an appropriate response to the changes in the operating modes. Since the STS is open, logically, the injected current goes to zero.

Case 3: At 0.6s, the grid's problem is solved and its voltage goes back to the acceptable range. As a result the STS is closed (GT mode) and the system is reconnected and synchronized to the main grid using a synchronous reference frame PLL [18]. In this condition, the reference value of the voltage controller is dictated by the voltage value at PCC. According to the smooth transition algorithm, the current controller will be the dominant controller (Section. III.E). Fig.8 and Fig.10.b are

representing the corresponding grids' current and the PCC voltage waveforms when the inverter's mode is changed from islanded to GT mode. These results indicate a smooth transition between these two operational modes.

Fig. 10.a) PCC voltage after inverter goes to the islanded mode from the GT mode at 0.4s. b) PCC voltage after inverter goes from the islanded mode to the GT mode at 0.6s

Fig. 11 shows the reference vs actual values of the I_d and I_q in GT mode. Optimizing the PIR controller parameters, the reference values are perfectly followed by the actual signals.

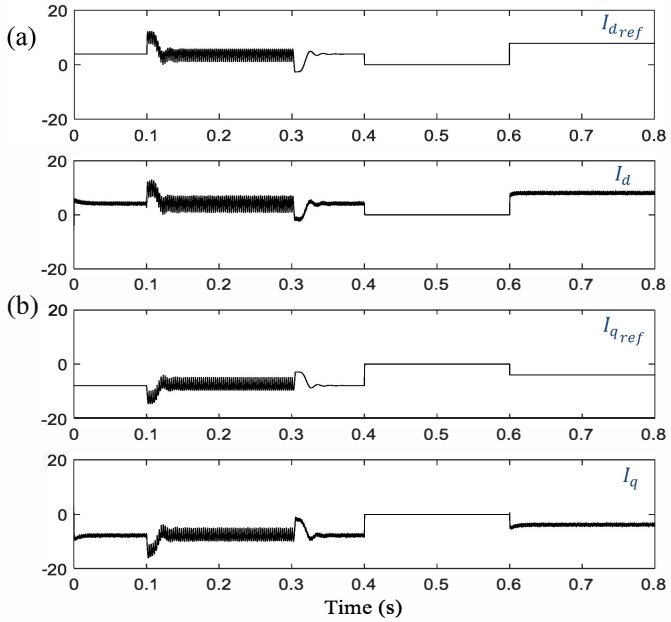

Fig.11. a) Comparison between I_d and I_{dref} and, b) Comparison between I_q and I_{qref}.

B. *Experimental Work*

This section contains the experimental work results for the proposed MFDMI. The overall system was modelled using a real-time simulator OPAL-RT (32 port OP5312), while all of the controllers have been realized using Texas instrument 595-TMS320F28335ZJZA (Digital Signal Processors & Controllers - DSP, DSC), Fig.7. Fig.12.a represents the voltage and injected current to the grid at PCC without harmonic compensation (where i_{d1}^* and i_{q1}^* are not considered in the controlling signal). Fig.12.b illustrates the same quantities with the harmonic compensation (10)-(11).

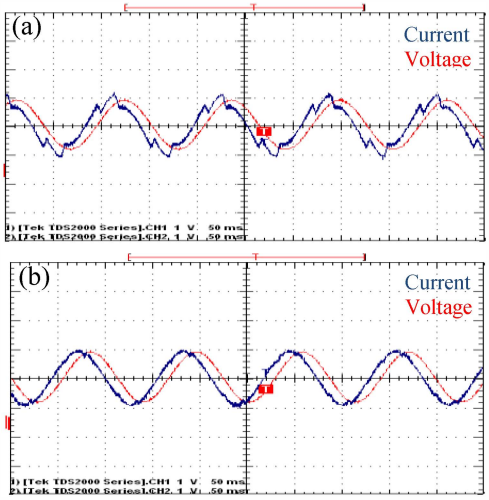

Fig.12. Voltage and injected current (pu) to the grid at PCC a) without harmonic compensation, and b) with harmonic compensation (Section III.A).

Fig. 13.a and b represent the MFDMI performance once the operational mode is changed from GT to Islanded and vice-versa, respectively. We can see the fast and smooth transition between two modes while the voltage and current signals (pu) are adjusted to the new modality of the system quickly and stably. Finally, we have shown the behavior of the power signals under GT mode (at PCC) vs their reference values in Fig.14. Using the proposed control approach, both the active and reactive powers can follow their reference values within a suitably stable and reliable behavior. Simulations in addition to experimental work results are indicating the adequate performance of the proposed MFDMI under different operational modes while satisfying the targeted goals, which have been listed in Section II.

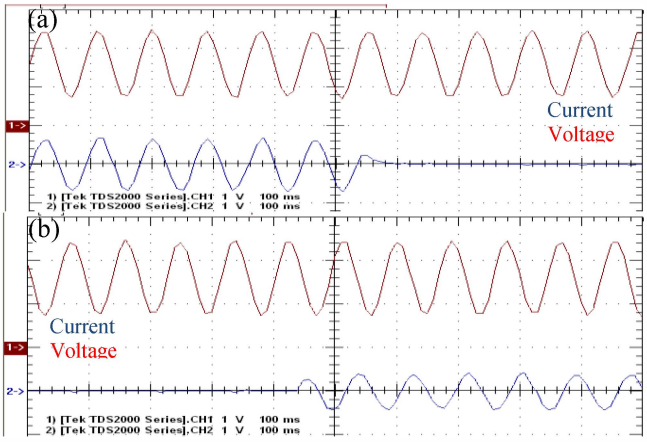

Fig.13. Voltage and injected current (pu) at the PCC after changing control method from a) GT to islanded, b) islanded to GT mode.

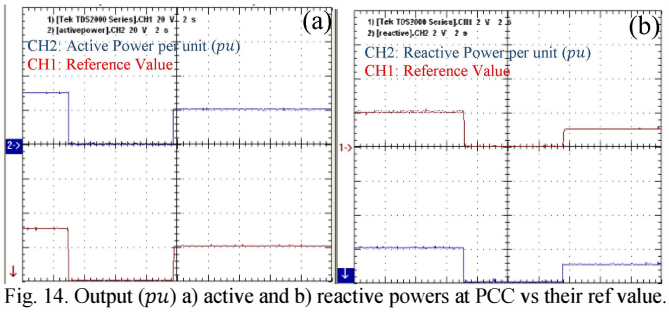

Fig. 14. Output (pu) a) active and b) reactive powers at PCC vs their ref value.

V. CONCLUSION

In this work a multi-functional double mode (GT/Islanded) inverter (MFDMI) is proposed for PV-based smart-grid applications, which is able to operate in different operational modes. Within the control framework, a new instantaneous d-q rotating reference frame-based Islanded detection approach has been initialized. Moreover, within each operational mode the reference control signals were obtained by means of the instantaneous power theory that improves the time efficiency due to time domain calculations. Floating interleaved converters are applied to address the PV module low output voltage issue. To increase the system reliability an energy storage system is also integrated. Moreover, using a unified control scheme the system reached to a very smooth transition between GT and islanded modes. In this paper, a PIR controller in implemented to perfectly handle the controlling tasks in the presence of harmonical nonlinear loads, PV output fluctuation and system switching. The proposed MFDMI could handle variety of operational challenges by injecting active and reactive powers to the grid as well as compensating harmonics of nonlinear loads and stabilizing the voltage at PCC. Experimental and simulation results indicate an appropriate performance of the proposed MFDMI under a variety of situations, supporting successful hardware implementation.

ACKNOWLEDGMENT

Authors would like to recognize helps and support from ACEPS lab former members, A. Reznik, and C. Lute.

REFERENCES

[1] S. Parhizi, H Lotfi, A. Khodaei, and Sh. Bahramirad. “State of the art in research on microgrids: a review”. *Access, IEEE* 3 (2015): 890-925.

[2] X. Yu, C. Cecati, T. Dillon, M. G. Simões “The new frontier of smart grids”. *IEEE Industrial Electronics Magazine*, Dec 2011, pp. 49-63, vo. 5, no. 3.

[3] M. Davoudi, V. Cecchi, and J. Romero Agüero, “Increasing penetration of distributed generation with meshed operation of distribution systems,” *North American Power Symposium (NAPS)*, Sept. 2014.

[4] M.G. Simões, T.C. Busarello, A.S. Bubshait, F. Harirchi, J.A. Pomilio, and F. Blaabjerg. "Interactive smart battery storage for a PV and wind hybrid energy management control based on conservative power theory." International Journal of Control (2015): 1-21.

[5] T.C. Busarello and J. Antenor Pomilio, “Bidirectional multilevel shunt compensator with simultaneous functionalities based on the conservative power theory,” in Proc. of PEMD, pp. 1-6, Apr. 2014.

[6] Varaprasad, O.V.S.R. and Sarma, D.V.S.S, “An improved SVPWM based shunt active power filter for compensation of power system harmonics”. *In Harmonics and Quality of Power (ICHQP), IEEE 16th International Conference on*. Pp: 571-575, 2014.

[7] Guzman, Ramon, et al. "Model-Based Control for a Three-Phase Shunt Active Power Filter.", *IEEE Trans on Industrial Electronics* 2016.

[8] A. Reznik, M. Godoy Simões, A. Al-Durra, S,M.Muyeen, "LCL filter design and performance analysis for grid interconnected systems" *IEEE Trans. on Industry Appl*., vol. 50, no.2, pp.1225-1232, Mar-Apr 2014.

[9] Y. Tang, P. C. Loh, P. Wang, F. H. Choo, and F. Gao, “Exploring inherent damping characteristic of LCL-filters for three-phase grid-connected voltage source inverters,” *IEEE Trans. Power Electron*., vol. 27, no. 3, pp. 1433–1443, Mar. 2012.

[10] N. He, D. Xu, Y. Zhu, J. Zhang, G. Shen, Y. Zhang, J. Ma, and C. Liu, “Weighted average current control in a three-phase grid inverter with an LCL filter,” *IEEE Trans. Power Electron*., vol. 28, no. 6, pp. 2785–2797, Jun. 2013.

[11] Z. Zeng, H. Yang, S. Tang, and R. Zhao, “Objective-oriented power quality compensation of multifunctional grid-tied inverters and its application in microgrids,” *IEEE Trans. Power Electron*., vol. 30, no. 3, pp.1255-1265, Mar. 2015.

[12] Z. Zeng, R. Zhao, H. Yang, and C. Cheng, “Topologies and control strategies of multi-functional grid-connected inverters for power quality enhancement: A comprehensive review,” *Renewable Sustainable Energy Rev*., vol. 24, pp. 223–270, Aug. 2013.

[13] Z. Zou, Z.Wang, and M. Cheng, “Modeling, analysis, and design of multifunction grid-interfaced inverters with output LCL filter,” *IEEE Trans. Power Electron*., vol. 29, no. 7, pp. 3830–3839, Jul. 2014.

[14] Z. Zeng, R. X. Zhao, and H. Yang, “Coordinated control of multifunctional grid-tied inverters using conductance and susceptance limitation,” *IET Power Electron*., 2014.

[15] TC. Busarello, J.A Pomilio, and M.G Simoes. "Passive Filter Aided by Shunt Compensators based on the Conservative Power Theory". *IEEE Trans on Industry Applications*. 2016.

[16] F.Harirchi, M.G.Simoes, A.Aldurra, S.M.Muyeen “Short Transient Recovery of Low Voltage Grid-Tied DC Distributed generation”. *IEEE ECCE*, pp: 1149-1155, 2015.

[17] F.Harirchi, M.G.Simões, M.Babakmehr, A.AlDurra, S,M.Muyeen, “Designing Smart Inverter with Unified Controller and Smooth Transition between Grid-Connected and Islanding Modes for Microgrid Application”, pp:1-7, *IEEE Indusry Appl Society (IAS)* GM, 2015.

[18] Morstyn, T., Hredzak, B., Demetriades, G. D., & Agelidis, V.G. Unified distributed control for dc microgrid operating modes. *Power Systems, IEEE Transactions on*, 31(1), 802-812, 2016.

[19] Hu, S. H., Kuo, C. Y., Lee, T. L., & Guerrero, J. M. Droop-controlled inverters with seamless transition between islanding and grid-connected operations. In Energy Conversion Congress and Exposition (ECCE), IEEE (pp. 2196-2201) 2011.

[20] Rahimi, Kaveh; Mohajeryami, Saeed; Majzoobi, Alireza, "Effects of Photovoltaic Systems on Power Quality," accepted and to be appeared in *North American Power Symposium (NAPS)*, 2016, Denver, USA.

[21] B. Singh, R. Niwas “Power Quality Improvement of PMSG-Based DG Set Feeding Three-Phase Loads” *IEEE Trans. Industry Applications*, Volume. 52, pp. 466 – 471, 2016.

[22] H. Akagi, E. H. Watanabe, and M. Aredes, “The Instantaneous power theory in Instantaneous power theory and applications to power conditioning”, pp. 75-79, *John Wiley & Sons, Inc*., New Jersey, 2007.

[23] A.Ramkumar, S.Durairaj, N.Arun “Comparison of PI and PIR Regulators for DFIG During Unbalanced Grid Voltage Conditions” *Power electronics and renewable energy systems*, Elsevier, 2015.

[24] Quan, X., Dou, X., Wu, Z., Hu, M., & Yuan, J. “Harmonic voltage resonant compensation control of a three-phase inverter for battery energy storage systems applied in isolated microgrid”. *Electric Power Systems Research*, 131, 205-217 (2016).

[25] Anderson, Paul M., and Aziz A. Fouad. “Power system control and stability”. *John Wiley & Sons*, 2008.

[26] Ko, W. H., & Gu, J. C. “Impact of shunt active harmonic filter on harmonic current distortion of voltage source inverter-fed drives”. *IEEE Transaction on Industry Applications* vol. 52, no. 4, Jul/Aug 2016.

[27] M. Babakmehr, M. Simoes, F. Harirchi, A. Alsaleem, A. Bubshait. “Designing an Intelligent Low Power Residential PV-Based Microgrid”, to be appeared in 51th *IEEE Industry Application Society General Meeting*, IAS 2016, Portland, USA.